Available online at www.sciencedirect.com
ScienceDirect
Composites: Part B 39 (2008) 50–56
composites Part B: engineering
www.elsevier.com/locate/compositesb

Helium permeability of coated aramid papers

Monika Bubacz [a,b,*], Andrey Beyle [b], David Hui [a], Christopher C. Ibeh [b]

[a] Department of Mechanical Engineering, University of New Orleans, New Orleans, LA 70148, USA
[b] Center for Nanocomposites and Multifunctional Materials [CNCMM], Pittsburg State University, Pittsburg, KS 66762, USA

Available online 17 February 2007

Abstract

Materials and technologies for cryogenic tanks design are still in the developmental stage. New design concepts demand that composite structure not only carries mechanical loads but provides hermetism. This paper aims at defining a cryogenic tank concept design and developing a barrier layer with impregnated aramid paper to prevent permeation of gases through a composite sandwich wall of the tank. A number of aramid fiber paper sheets have been coated with different resin systems and tested for helium permeability. Permeation kinetics show that there are at least two mass transport mechanisms running simultaneously: diffusion and hydrodynamic flow through micro-porous media. The long period of unsteady permeability was determined. Despite some technological imperfections of the laboratory-made samples, a low level of permeability was achieved, which satisfied the official requirements. Both steady level of permeability and kinetics of unsteady period can be used for quality control purposes.

Keywords: A. Aramid fiber; A. Honeycomb; A. Resins; Permeability

1. Introduction

Fiber reinforced plastics offer the advantage of specific strength and stiffness compared to metals and have been identified as candidates for reusable space transportation systems. Materials and technologies for cryogenic tank design, which are capable of meeting the flight requirements in a harsh environment, are still under development. A number of carbon and aramid fiber reinforced plastics are considered and the material selection is based on mechanical properties, containment performance (long and short term), and manufacturing considerations. Lifetime durability requirements for cryogenic fuel tanks imply that the materials must safely carry pressure, external structural loads, resist leakage, and operate over an extremely wide temperature range [1]. The rate of gas leakage can be a function of material, tank fabrication method, mechanical load to the tank, internal damage-state of the material, and the temperatures at which the tank must operate [2]. Conventional concept of cryogenic tank includes metallic liners fulfilling mainly hermetism function. A liner is enclosed in a composite structure carrying main mechanical loads. However, experiments show that reliability of welded joints of metallic liners is insufficient for harsh environments and the composite structure also has to fulfill hermetic function. Usually, composites have sets of micro-cracks which are not permeable for liquids but are permeable for small molecules of gases, such as hydrogen or helium. The goal of the present research is to radically decrease permeability of composites with respect to the gases. So far, IM7/977-2 (graphite-epoxy) skin layers and Kevlar (aramid) honeycombs were chosen as the most promising and reliable materials, and thin polymer films were introduced between layers in the composite to form an interleaved or hybrid composite, and to decrease the permeability. The effects of the layer thickness, number, and location on the mechanical properties of the laminate were investigated [3].

* Corresponding author. Address: Center for Nanocomposites and Multifunctional Materials [CNCMM], Pittsburg State University, Pittsburg, KS 66762, USA. Tel.: + 1 504 3520297; fax: +1 620 2354004.
E-mail address: mbubacz@uno.edu (M. Bubacz).

1359-8368/$ - see front matter © 2007 Elsevier Ltd. All rights reserved.
doi:10.1016/j.compositesb.2007.02.004

The objective of this research is to study the effects of various design, manufacturing, and service parameters on the susceptibility of composite tanks to excessive permeability of cryogenic fuels. This research considers using non-symmetrical composite sandwich structures with an inner wall to meet the cryogenic requirements. The main requirements for internal composite stack are: to reduce the wall permeability to hydrogen, to improve impact resistance, and to prevent micro-cracking, crack propagation, and subsequently gas permeability by introduction of barrier layer (e.g. aramid paper sheet, see Fig. 1). The structure may incorporate nanoparticles for properties modification and barrier development. Clays and inorganic reinforcements have been shown to be effective reinforcements in neat polymeric structures [4–6]. Results of influence of nanoinclusions on gas permeability will be published in the future.

Though addition of film interleaves into composite laminates increases the resistance to fatigue and impact of the composite, it also reduces the specific strength of the material due to increased part weight, which is unacceptable in weight-critical applications such as reusable launch vehicles. Film used only as a barrier creates a surface of poor resistance to shear, transversal tension, delamination, and crack propagation. Aramid papers have much higher mechanical properties than polymer films and it is necessary to reduce their permeability by polymer impregnation. This additional resin coated layer, which is compatible to honeycomb material, can be integrated into the core structure and become an integral part. Fig. 1 depicts a new solution of closed cell honeycomb core to be tested. Novel nanocomposite materials made from nanoclay filled materials are currently under development for making barrier films. Such materials form lamellar structures that both increase the modulus of the polymer and provide additional barrier properties. The use of these materials may increase the overall specific strength of the material, while providing the permeation resistance.

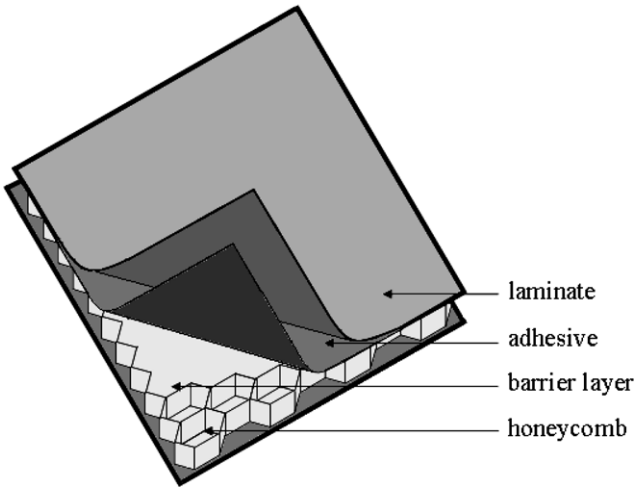

Fig. 1. Closed cell honeycomb sandwich structure.

It has been reported that the requirement adopted by National Aerospace Plane Program is that the allowable permeation rate is determined for the entire tank surface area as 10% of what will leak out of valves and fittings. This allowable flow rate per unit area is then calculated to be in the range of 0.01–0.1 Pa · m^2/s, at least two orders of magnitude greater than the discriminating value (currently minimum detectable or 0.003 Pa · m^2/s). Furthermore, depending upon the failure mode and representative vehicle configuration, realistic hydrogen flow rate allowable ranges from 0.36 to 900 Pa · m^2/s [7].

2. Permeability phenomenon

In the case of current permeability measurements, values obtained from helium leak detector characterize a flow rate or leak rate Q, and after taking into consideration area A of flow, this value is recalculated to permeation rate, which characterizes flow rate density q_{pV} or pV flow per unit area. Permeability coefficient called simply permeability K_{pV} can be obtained from the empirical linear law:

$$K_{pV} = q_{pV}\frac{h}{\Delta p} = \frac{Q_{pV}}{A}\frac{h}{\Delta p} \tag{1}$$

Distribution of pressures through the membrane of thickness h, where on one side the pressure is constant and equal p_1, on the other the pressure p_2 is equal zero ($p_1 = \Delta p$), also initial pressure is equal zero, can be described by following equation (derivation in terms of diffusion [9]):

$$\frac{p}{\Delta p} = 1 - \frac{x}{h} - \frac{2}{\pi}\sum_{n=1}^{\infty}\frac{1}{n}\sin\frac{n\pi x}{h}\exp\left(-\frac{K_{pV}n^2\pi^2 t}{h^2}\right) \tag{2}$$

Flux (per unit area) in a non-steady process can be obtained from:

$$q_{pV} = -K_{pV}\frac{\mathrm{d}p}{\mathrm{d}x} = K_{pV}\frac{\Delta p}{h}\left[1 + 2\sum_{n=1}^{\infty}\cos\frac{n\pi x}{h}\exp\left(-\frac{K_{pV}n^2\pi^2 t}{h^2}\right)\right] \tag{3}$$

At the opposite side of the membrane (at $x = h$) there is:

$$q_{pV} = K_{pV}\frac{\Delta p}{h}\left[1 + 2\sum_{n=1}^{\infty}(-1)^n\exp\left(-\frac{K_{pV}n^2\pi^2 t}{h^2}\right)\right] \tag{4}$$

The results of calculations according to this formula, written in dimensionless form, are plotted in Fig. 2. This graph can be used for finding permeability coefficient for both steady and unsteady state.

The first derivative of the flux is:

$$\frac{\mathrm{d}q_{pV}}{\mathrm{d}t} = -K_{pV}\frac{\Delta p}{h}2\left[\sum_{n=1}^{\infty}(-1)^n\frac{K_{pV}n^2\pi^2}{h^2}\exp\left(-\frac{K_{pV}n^2\pi^2 t}{h^2}\right)\right] \tag{5}$$

and the graph of this function in dimensionless form is shown in Fig. 3.

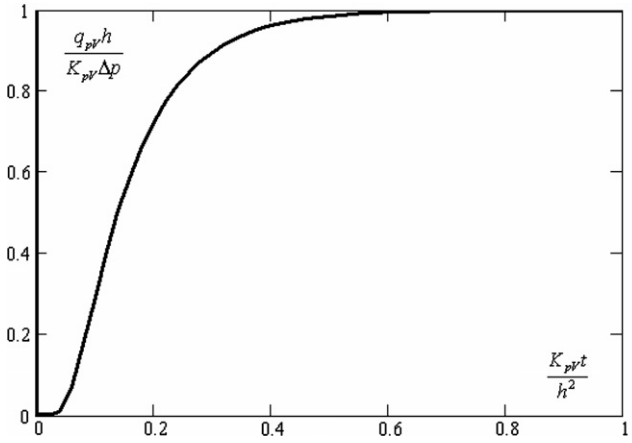

Fig. 2. Dimensionless graph of flow density calculated analytically.

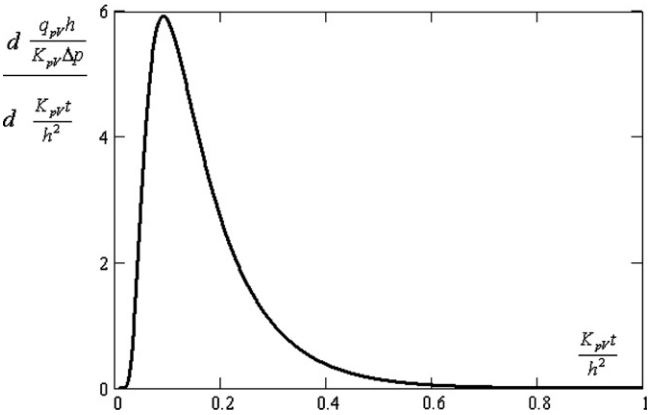

Fig. 3. Dimensionless graph of first derivative of flow density.

The second derivative is:

$$\frac{\mathrm{d}^2 q_{pV}}{\mathrm{d}t^2} = K_{pV}\frac{\Delta p}{h}2\left[\sum_{n=1}^{\infty}(-1)^n \frac{K_{pV}^2 n^4\pi^4}{h^4}\exp\left(-\frac{K_{pV}n^2\pi^2 t}{h^2}\right)\right] \tag{6}$$

and the graph of this function in dimensionless form is shown in Fig. 4.

The inflection point (point of maximum of the first derivative) can be used to determine the permeability coefficient in unsteady process. Let's denote the maximal value of the derivative as $L = \max\left(\frac{\mathrm{d}q_{pV}}{\mathrm{d}t}\right)$ and corresponding time as t^*. Then permeability coefficient can be calculated from:

$$K_{pV} = \sqrt{\frac{L}{5.922}\frac{h^3}{\Delta p}} \tag{7}$$

$$\text{or } K_{pV} = 0.09175\frac{h^2}{t^*} \tag{8}$$

Total quantity of pV passed through unity of membrane area from the beginning up to current time t can be calculated from:

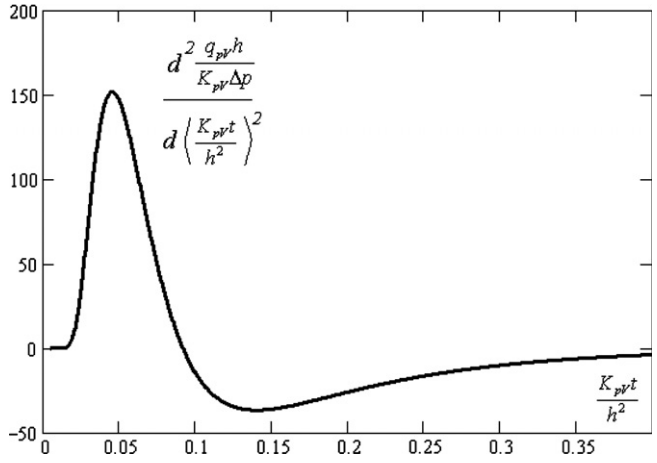

Fig. 4. Dimensionless graph of second derivative of flow density.

$$\begin{aligned} Z_{pV} &= \int_0^t q_{pV}\mathrm{d}t \\ &= K_{pV}\frac{\Delta p}{h}\int_0^t\left[1+2\sum_{n=1}^{\infty}(-1)^n\exp\left(-\frac{K_{pV}n^2\pi^2 t}{h^2}\right)\right]\mathrm{d}t \\ &= K_{pV}\frac{\Delta p}{h}\left\{t-2\sum_{n=1}^{\infty}(-1)^n\frac{h^2}{K_{pV}n^2\pi^2}\right. \\ &\quad\left.\times\left[\exp\left(-\frac{K_{pV}n^2\pi^2 t}{h^2}\right)-1\right]\right\} \end{aligned} \tag{9}$$

or, since $\sum_{n=1}^{\infty}(-1)^n\frac{1}{n^2} = -\frac{\pi^2}{12}$ [8], it can be obtained from:

$$\begin{aligned} Z_{pV} &= K_{pV}\frac{\Delta p}{h}\left[t-\frac{2h^2}{\pi^2 K_{pV}}\sum_{n=1}^{\infty}(-1)^n\frac{1}{n^2}\right. \\ &\quad\left.\times\exp\left(-\frac{K_{pV}n^2\pi^2 t}{h^2}\right)-\frac{h^2}{6K_{pV}}\right] \\ &= h\Delta p\left[-\frac{1}{6}+\frac{K_{pV}}{h^2}t-\frac{2}{\pi^2}\sum_{n=1}^{\infty}\frac{(-1)^n}{n^2}\exp\left(-\frac{K_{pV}n^2\pi^2 t}{h^2}\right)\right] \end{aligned} \tag{10}$$

and matches well-known formula [9].

At the end of the process this dependence becomes an asymptotic straight line:

$$Z_{pV} = K_{pV}\frac{\Delta p}{h}\left[t-\frac{h^2}{6K_{pV}}\right] = h\Delta p\left[-\frac{1}{6}+\frac{K_{pV}}{h^2}t\right] \tag{11}$$

When this straight line intercepts the abscissa $Q_{pV} = 0$, the time $t = t^{\wedge}$ corresponds to:

$$-\frac{1}{6}+\frac{K_{pV}}{h^2}t^{\wedge} = 0 \tag{12}$$

$$\text{or } K_{pV} = \frac{h^2}{6t^{\wedge}} \tag{13}$$

This intercept (time lag) can be used for permeability coefficient determination as well as the slope of the asymptotic straight line, Fig. 5:

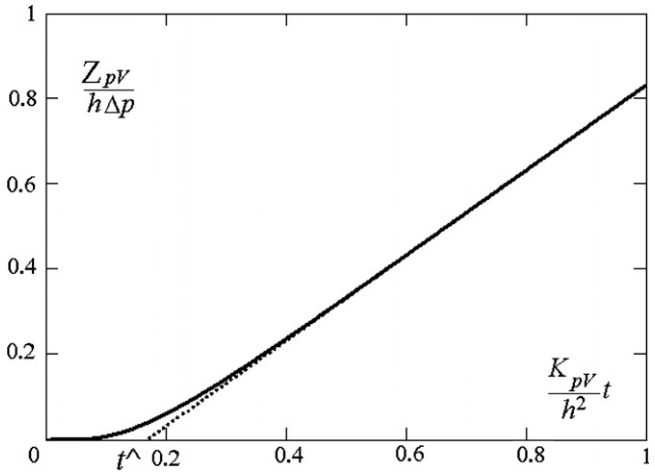

Fig. 5. Different approach to steady-state flow through a membrane.

$$\frac{dZ_{pV}}{dt} = K_{pV}\frac{\Delta p}{h} \quad \text{at } t \to \infty \tag{14}$$

and

$$K_{pV} = \frac{h}{\Delta p}\left(\frac{dZ_{pV}}{dt}\right)_{t\to\infty} \tag{15}$$

Using differential procedures in an experiment requires suppressing of all the side effects (in this case – creep of the membrane, slow sliding of the membrane from the clamps, all sources of leakage or bypassing, etc.). If the level of "the statistical noise" is two high, application of differential procedures becomes impossible.

3. Experimental procedure

Samples of skin and core material with different resin systems were tested for helium gas permeability using a helium mass spectrometer and a specially designed and manufactured sample fixture. Nomex 3T412 and Kevlar 2.8N636 aramid papers from DuPont were coated with unsaturated polyester Bondo 7630800402 from Dynatron/Bondo Corp., fiberglass polyester resin NAPA 765-1286 from Balkamp, Inc., both mixed with 1.5% of methyl ethyl ketone peroxide (MEKPO), low viscosity epoxy MAS 30-002 mixed with fast epoxy hardener MAS 30-012, and medium–low viscosity SilverTip Marine Epoxy laminating resin with fast hardener from System Three Resins, Inc. Alcohol and acetone were added as diluents for temporary decreasing of viscosity during impregnation process, for easier penetration into narrow micro-channels between fibers, and for decreasing of thickness of pure polymer layer over aramid papers. Resin was applied with brush or rollers to both sides of papers and cured in a press between metal plates at room temperature or in a vacuum-bag in oven (different processes for different trials in order to obtain the best quality of samples). Helium permeability tests were performed on 4–8 samples (depending on repeatability) in a specially built set-up with gaseous helium as a permeant using Alcatel ASM 142, an universal helium leak detector with usable helium sensitivity in the 10^{-6} Pa · cm^3/s range. The helium was pumped with stable pressure 6.9 and 34.5 kPa. The thickness differed for different trials and different coating processes. Sample nomenclature is explained in Table 1.

Table 1
Sample nomenclature

Symbol	Explanation	Remarks Test inlet pressure P [kPa] Average thickness h [mm]
N1	Nomex 3T412 uncoated	$P = 6.9$, $h = 0.076$
N2	Nomex 2T412 uncoated	$P = 6.9$, $h = 0.051$
NP2	Nomex 3T412 coated with unsaturated polyester Bondo	Trial 2, almost no resin $P = 6.9$, $h = 0.076$
NP3	Nomex 3T412 coated with unsaturated polyester Bondo	Trial 3, paper partially coated, air bubbles $P = 34.5$, $h = 0.381$
NP4	Nomex 3T412 coated with unsaturated polyester Bondo	Trial 4, very uneven coating, cracked, falls off $P = 6.9$, $h = 0.076$
KP1	Kevlar 2.8N636 coated with unsaturated polyester Bondo	Trial 1, small air bubbles on one side $P = 34.5$, $h = 0.279$
KP2	Kevlar 2.8N636 coated with unsaturated polyester Bondo	Trial 2, paper stuck to nylon film, thin coating $P = 34.5$, $h = 0.152$
KP3	Kevlar 2.8N636 coated with unsaturated polyester Bondo	Trial 3, uneven coat surface, wrinkles $P = 34.5$, $h = 0.229$
KP4	Kevlar 2.8N636 coated with unsaturated polyester Bondo	Trial 4, very thick coating, big air bubbles $P = 34.5$, $h = 0.432$
NF1	Nomex 3T412 coated with fiberglass polyester resin NAPA	Trial 1 $P = 34.5$, $h = 0.152$
NF2	Nomex 3T412 coated with fiberglass polyester resin NAPA	Trial 2, alcohol added as diluent $P = 34.5$, $h = 0.279$
KF1	Kevlar 2.8N636 coated with fiberglass polyester resin NAPA	Trial 1, alcohol added as diluent $P = 34.5$, $h = 0.127$
NE1	Nomex 3T412 coated with low viscosity epoxy MAS	Trial 1 $P = 34.5$, $h = 0.102$
KE1	Kevlar 2.8N636 coated with low viscosity epoxy MAS	Trial 1, alcohol added as diluent $P = 34.5$, $h = 0.279$
KE2	Kevlar 2.8N636 coated with low viscosity epoxy MAS	Trial 2, more alcohol added as diluent $P = 34.5$, $h = 0.127$
NM1	Nomex 2T412 coated with marine epoxy	Trial 1 $P = 34.5$, $h = 0.417$
NM1a	Nomex 2T412 coated with marine epoxy, different sample	Trial 1a $P = 34.5$, $h = 0.354$
NM2	Nomex 2T412 coated with marine epoxy	Trial 2, acetone added as diluent $P = 34.5$, $h = 0.164$
KM1	Kevlar 3.9N636 coated with marine epoxy	Trial 1 $P = 34.5$, $h = 0.455$
KM2	Kevlar 3.9N636 coated with marine epoxy	Trial 2, acetone added as diluent $P = 34.5$, $h = 0.487$

4. Results and discussion

Nomex T412 has low permeability without the resin coating, while Kevlar N635 paper is saturable and porous. As a consequence, resin will penetrate Kevlar paper, giving a non-porous system. It was impossible to test Kevlar paper because the permeability machine was not able to create a vacuum between the sample and mass spectrometer. Nomex paper with two different thicknesses was tested under helium pressure of 6.9 kPa. First tests on Nomex 3T412 were performed under unstable inlet pressure due to the big rate of gas flow through the sample and difficulties with keeping the inlet pressure at one level as shown in Fig. 6. Flow rate values received from the helium leak detector every 30 s were recalculated to obtain a flow rate density for this particular sample fixture taking flow area dimensions into consideration.

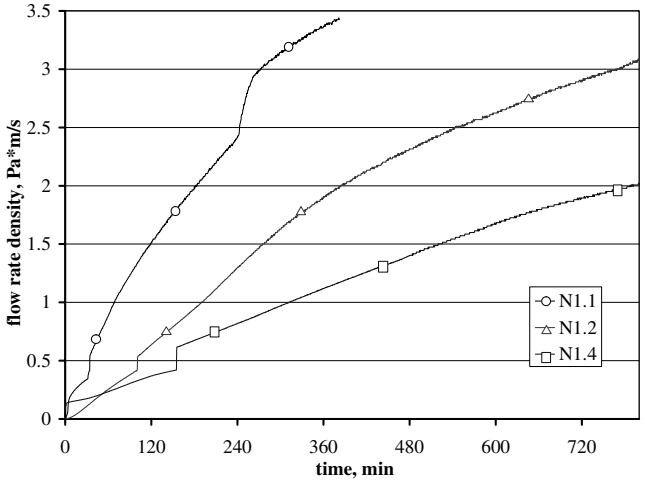

Fig. 6. Flow rate density q_{pV} of uncoated Nomex.

Tests showed that thicker papers have lower permeability rates. This agrees with the linear law of flow (1), which states that permeability depends on and is inversely proportional to the thickness. Time of stabilization also depended on the specimen dimension. For thicker samples it takes more time to stabilize the permeation rate because the sorption and desorption processes last longer.

All coated samples were tested under pressure of 34.5 kPa. Fig. 7 depicts results for Nomex coated with polyester, which retained a relatively uniform thickness and smooth coating. The manufacturing process gave small air bubbles on one of the surfaces and the defect amount differs for each sample, with the smallest count for NP3.3 and NP3.5. These samples had a flow rate density, which did not exceed 5×10^{-5} Pa m^2/s and stabilized within first hour.

A roller (iron) was used after applying resin with a brush to better impregnate pores in Kevlar paper, and a very thick coating with infrequent big air bubbles was obtained. Samples with undamaged surfaces and without visible pores were chosen and tested. Fig. 8 shows graphs with smooth curves which achieved steady level of flow rate within approximately 6–8 h.

Similar tests were performed for Nomex and Kevlar papers coated with fiberglass polyester and epoxy. The tests demonstrated that aramid paper sheets coated with a resin system satisfies the requirements adopted by National Aerospace Plane Program and can be used as an interleaf in the sandwich structure to improve the mechanical properties of the whole structure with sustainable high gas pressure capability. Nomex T412 paper showed better permeability resistance than Kevlar N635 and stabilized faster. In all shown test results, the unsteady stage of the process dominated. It is characterized by a more wide statistical range than steady state. A comparison of permeability coefficient K_{pV} for samples from different trials is shown in Fig. 9 and contains an average and a standard

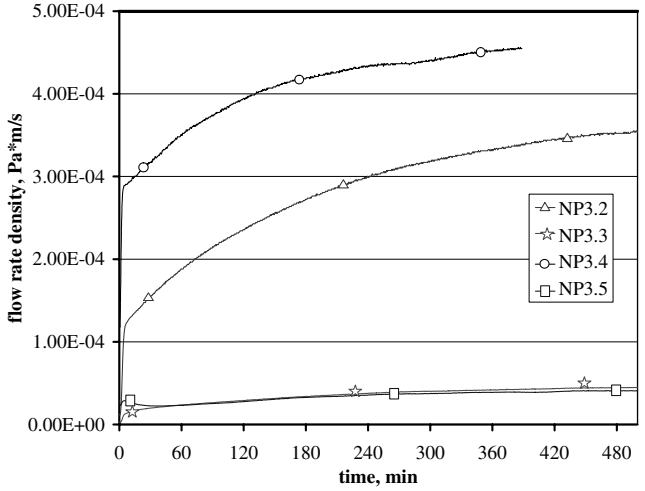

Fig. 7. Flow rate density q_{pV} of Nomex coated with polyester.

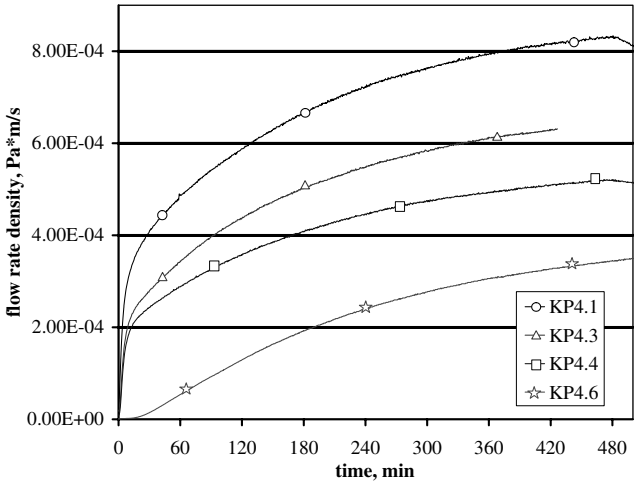

Fig. 8. Flow rate density q_{pV} of Kevlar coated with polyester.

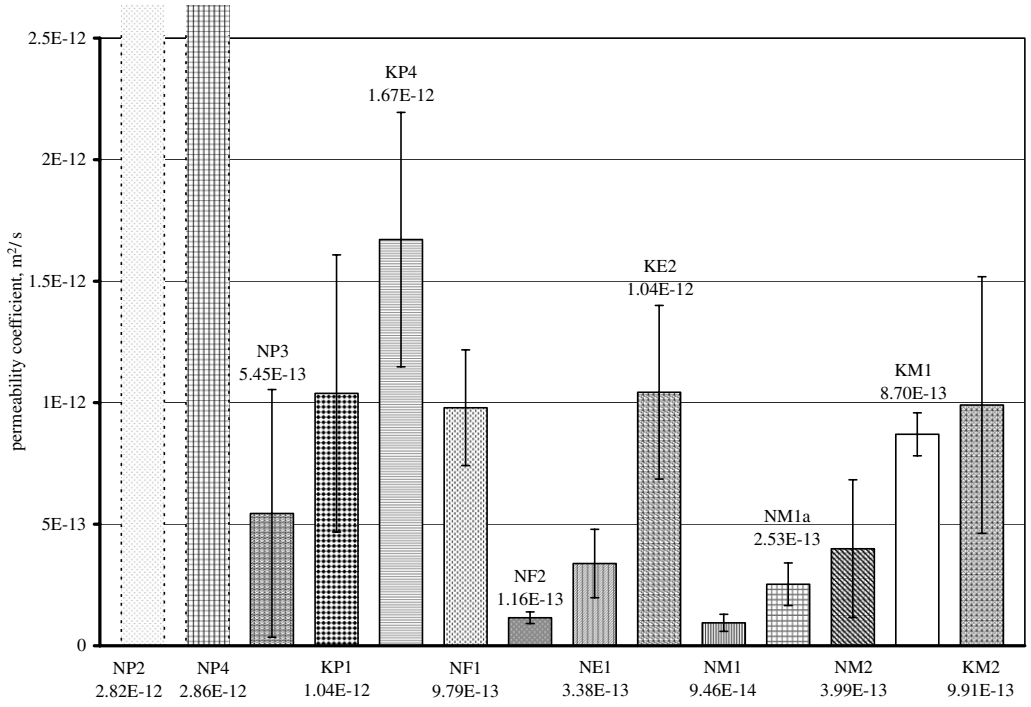

Fig. 9. Comparison of permeability of coated paper.

deviation of results. Samples of Nomex coated with polyester in trials 2 and 4 had coating, which fell off but left resin residue on surface and improved helium permeability resistance. Those samples were tested with inlet pressure 6.9 kPa because of samples fragility. The smallest deviation is found to belong to the trial with the smallest permeability coefficient value (for Nomex coated with fiberglass polyester resin), which means that those samples had a very uniform and good quality coating.

Addition of acetone caused increase in both permeation rate and permeability coefficient. It can be observed for samples of papers coated with unsaturated polyester: Nomex when comparing NP2 to NP4, Kevlar when comparing KP1 to KP3 and KP4. It is strongly visible for samples of marine epoxy SilverTip and papers coated with it. Addition of alcohol gave opposite outcome: decrease of permeation. It can be observed for samples of Nomex coated with fiberglass polyester when comparing NF1 to NF2 and for Kevlar coated with epoxy MAS when KE2 with bigger amount of alcohol has smaller permeability coefficient than KE1.

Table 2 shows comparison of permeability coefficient obtained from steady state part of leak rate curves and calculations based on derivatives and integrals of these curves. $K(L)$, $K(t^*)$, $K(Z')$, and $K(t\hat{})$ were calculated using Eqs. (7), (8), (15) and (13), respectively. The closest values of K were obtained from calculations based on L, which is the maximal value of the derivative, obtained from the beginning of the process. But it is still not as precise as traditional method and long-term testing procedure should not be neglected. Calculation of $K(Z')$ and $K(t\hat{})$ gave much smaller values and should not be considered as a trustful method for calculating permeability coefficient.

All methods used for determination of permeability coefficients have their own negative sides and the results do not match well. It is necessary to mention that determination of low permeability is not easy: some defects or their configurations among parallel samples can change the

Table 2
Comparison of permeability coefficients $K[m^2/s]$ obtained from different sources

Sample	K	$K(L)$	$K(t^*)$	$K(Z')$	$K(t\hat{})$
NP4.1	1.55×10^{-10}	1.46×10^{-11}	7.1×10^{-12}	4.9×10^{-12}	1.26×10^{-13}
NP4.2	2.1×10^{-10}	2.35×10^{-11}	2.54×10^{-12}	7.05×10^{-12}	2×10^{-13}
KF1.1	1.34×10^{-12}	3×10^{-12}	1.93×10^{-11}	4.4×10^{-14}	8.21×10^{-13}
KF1.2	1.15×10^{-12}	3.08×10^{-12}	3.7×10^{-11}	3.8×10^{-14}	1.11×10^{-12}
KF1.3	8.08×10^{-13}	1.85×10^{-12}	2.47×10^{-11}	2.6×10^{-14}	4.74×10^{-13}
KF1.4	9.37×10^{-13}	2.16×10^{-12}	1.71×10^{-11}	3.03×10^{-14}	5.16×10^{-13}
KE2.1	1.45×10^{-12}	2.16×10^{-12}	8.88×10^{-12}	5.02×10^{-14}	3.9×10^{-13}
KE2.3	8.67×10^{-13}	1.81×10^{-12}	1.41×10^{-11}	2.87×10^{-14}	3.54×10^{-13}
KE2.4	8.08×10^{-13}	1.62×10^{-12}	1.41×10^{-11}	2.73×10^{-14}	2.95×10^{-13}

value of permeability coefficient by several decimal orders. The main method used in this work was based on achieving steady state of permeation; however, this state is reached usually after several hours. Polymer membrane under even small difference of pressures can have significant creep during this time, which causes a change of structure of membrane material, and the change in defect configuration can significantly affect the results of permeability test. Methods based on differentiation of experimental kinetic curve usually have very low repeatability and small deviation of experimental results can give significant change in the slope of experimental curve. Methods based on using the specific time are also not good because the start time of the process is determined with some error related to the manual procedure. Time $t^{\wedge}$ is determined from extrapolation and depends on the slope of the curve. Time t^{*} is determined from the maximum of the slope, which is very sensitive to experimental errors. Comparison of results shows difference from few percents to change in decimal order. However, because the physical meaning of permeability coefficients found by different methods can vary (characteristic of initial structure of membrane, characteristic of structure after creep, characteristic of dynamics of structural change, etc.), the information obtained from different methods can be useful for analysis and for qualitative comparison of different materials.

5. Conclusions

The research described above proves that coated aramid papers are excellent candidates for barrier materials. Gas permeability has been tested through long-term leak rate control process and calculated using mathematical approach. The differential methods as well as the time lag method gave results which did not match well, while the most trustful method was the long-term gas leak testing procedure. It means that the method of the test and the nature of the tested sample give too high level of ''noise'' for application of differential methods. However, the information obtained from different methods can be used for comparison of different materials.

During sample preparation and permeability testing influence of sample manufacturing procedure on various properties was strongly visible. Diluents should be chosen to enhance resin properties; tests showed that acetone increases permeability coefficient while alcohol gives opposite effect.

Acknowledgements

This project was supported by ONR Grant No. 0601103N.

The authors would like to acknowledge Center for NanoComposites and Multifunctional Materials CNCMM at Pittsburg State University and ONR – Solid Mechanics Division for the support of current research, monitored by Dr. Yapa Rajapakse. Also, we would like to thank Robert A. Susnik, Pittsburg State University, Kansas, for help in sample manufacturing. Also, thanks to Dr. Carl Ventrice from University of New Orleans, Louisiana, for sample fixture machining and help with permeability equipment set-up. Special thanks to Hal Loken and Subhotosh Khan from DuPont for the supply of Kevlar and Nomex papers.

References

[1] Daniel L, Tumino G, Henriksen T, Dujarric C. Survey of advanced materials in Reusable Launch Vehicle (RLV).
[2] Rivers HK, Sikora JG, Sankaran SN. Detection of Micro-Leaks through complex geometries under mechanical load and at Cryogenic Temperature AIAA-2001-1218.
[3] Grimsley BW, Cano RJ, Johnston NJ, Loos AC, McMahon WM. Hybrid Composites for LH2 Fuel Tank Structure.
[4] Timmerman JF, Hayes BS, Seferis JC. Comp Sci Technol 2002;62:1249–58.
[5] Abdalla MO, Dean D, Campbell S. Polymer 2002;43:5887–93.
[6] Campbell S, Johnston JC, Inghram L, McCorkle L, Silverman E. NASA/TM-2003-212221 April 2003.
[7] Sparks S. Development of a Cryo-Biaxial permeability apparatus to measure the hydrogen permeability through composite cryotank materials and the generation of a database to aide in the selection of reusable composite cryotank materials.
[8] Gradshteyn IS, Ryzhik IM. Tables of integrals, series, and products. Academic Press; 1965.
[9] Crank J. The mathematics of diffusion. Oxford Science Publication; 1997.